Assimilation of POLDER aerosol optical thickness into the LMDz-INCA model: Implications for the Arctic aerosol burden

S. Generoso, Francois-Marie Breon, Fréderic Chevallier, Yves Balkanski, Michael Schulz, Isabelle Bey

Assimilation of POLDER aerosol optical thickness into the LMDz-INCA model: Implications for the Arctic aerosol burden

S. Generoso,[1,2] F.-M. Bréon,[1] F. Chevallier,[1] Y. Balkanski,[1] M. Schulz,[1] and I. Bey[3]

Received 5 December 2005; revised 26 August 2006; accepted 13 September 2006; published 31 January 2007.

[1] The large spatial and temporal variability of atmospheric aerosol load makes it a challenge to quantify aerosol effect on climate. This study is one of the first attempts to apply data assimilation for the analysis of global aerosol distribution. Aerosol optical thickness (AOT) observed from the Polarization and Directionality of the Earth Reflectances (POLDER) spaceborne instrument are assimilated into a three-dimensional chemistry model. POLDER capabilities to distinguish between fine and coarse AOT are used to constrain them separately in the model. Observation and model errors are a key component of such a system and are carefully estimated on a regional basis using some of the high-quality surface observations from the Aerosol Robotic Network (AERONET). Other AERONET data provide an independent evaluation of the a posteriori fields. Results for the fine mode show improvements, in terms of reduction of root-mean-square errors, in most regions with the largest improvements found in the Mediterranean Sea and Eurasia. We emphasize the results for the Arctic, where there is growing evidence of a strong aerosol impact on climate, but a lack of regional and continuous aerosol monitoring. The a posteriori fields noticeably well reproduce the winter-spring ''Arctic Haze'' peak measured in Longyearbyen (15°E, 78°N) and typical seasonal variations in the Arctic region, where AOT increase by up to a factor of three between a posteriori and a priori. Enhanced AOT are found over a longer period in spring 2003 than in 1997, suggesting that the large Russian fires in 2003 have influenced the Arctic aerosol load.

Citation: Generoso, S., F.-M. Bréon, F. Chevallier, Y. Balkanski, M. Schulz, and I. Bey (2007), Assimilation of POLDER aerosol optical thickness into the LMDz-INCA model: Implications for the Arctic aerosol burden, *J. Geophys. Res.*, *112*, D02311, doi:10.1029/2005JD006954.

1. Introduction

[2] Aerosols influence the Earth radiative budget through sunlight absorption and scattering to space (direct effect) and through their impacts on cloud microphysics and dynamics (indirect effects). Anthropogenic activities such as biomass burnings or industries mainly impact the fine fraction of aerosols, while natural sources release a majority of coarse particles (mostly dust and marine aerosols) in the atmosphere [e.g., *Kaufman et al.*, 2002]. The submicron particles have the most efficient effect on climate because of their radiative properties [*Intergovernmental Panel on Climate Change*, 2001], in addition they have longer residence time compare to the coarse particles. Quantifying the aerosol effects is essential for a global understanding of the anthropogenic impact on climate. Global models of aerosol chemistry and transport are particularly well suited to provide all the necessary information needed to quantify the aerosol impacts, but they still suffer from large uncertainties in source definitions, transport and removal processes. Satellite products provide unique observations of the atmospheric state, but they suffer from incomplete coverage and information. For instance, there is no aerosol detection in the presence of clouds; no information is yet available on the vertical distribution or on the chemical nature of the aerosol. In this context, a synergetic use of both models and satellites could help reduce present uncertainties, which is the essence of data assimilation. Such techniques have been used in atmospheric sciences first to improve weather forecast [*Le Dimet and Talagrand*, 1986; *Lorenc et al.*, 1991; *Courtier et al.*, 1994], and then to improve the representation of the distribution of trace gases [e.g., *Fisher and Lary*, 1995; *Khattatov et al.*, 1999; *Lamarque et al.*, 1999; *Clerbaux et al.*, 2001]. The first application to the study of aerosols is presented by *Collins et al.* [2001]. These authors assimilated the aerosol optical thickness (AOT) retrieved from Advanced Very High Resolution Radiometers (AVHRR) observations [*Stowe et al.*, 1997] into the Model of Atmospheric Transport and Chemistry (MATCH [*Rasch et al.*, 1997]) using Kalman filtering [*Kalman and Bucy*, 1961]. Their results were then used to provide improved aerosol distribution [*Rasch et al.*, 2001] and estimates of their direct radiative forcing [*Collins et al.*,

[1]Institut Pierre-Simon Laplace/Laboratoire des Sciences du Climat et de l'Environnement, Commissariat à l'Énergie Atomique–Centre National de la Recherche Scientifique, Gif-sur-Yvette, France.
[2]Now at Laboratoire de Modélisation de la Chimie Atmosphérique, Ecole Polytechnique Fédérale de Lausanne, Lausanne, Switzerland.
[3]Laboratoire de Modélisation de la Chimie Atmosphérique, Ecole Polytechnique Fédérale de Lausanne, Lausanne, Switzerland.

0148-0227/07/2005JD006954

2002] in the framework of the Indian Ocean Experiment (INDOEX) in spring 1999.

[3] In the present study, we combined AOT measured by Polarization and Directionality of the Earth Reflectances (POLDER) and simulated by the Laboratoire de Météorologie Dynamique–Interaction with Chemistry and Aerosol (LMDz-INCA) model to provide improved global distribution of aerosols. A particular emphasis was given to the quantification of the observation and model errors, using AOT ground-based measurements from the Aerosol Robotic Network (AERONET). These error statistics, which are crucial for the data assimilation system, were estimated at regional scale. Other data from this same network were also used to independently evaluate the a posteriori aerosol fields. Another specificity of the present study is the concomitant assimilation of fine and coarse mode satellite products. Current satellite measurements and retrieval techniques do not yet provide reliable information on the chemical properties of aerosols. However, fine and coarse mode products provide a useful indication on the aerosol nature as the largest anthropogenic sources are predominantly in the fine mode. *Kaufman et al.* [2005] recently used fine and coarse aerosol fraction retrieved from Moderate Resolution Imaging Spectroradiometer (MODIS) observations to provide an estimate of the anthropogenic AOT. Thus it is expected that the assimilation of the two aerosol modes separately will help quantifying the anthropogenic aerosol forcing on climate.

[4] Our approach to assimilate aerosol satellite data is described in section 2 and the a posteriori validations are presented in section 3. The results on the global aerosol distributions are presented in section 4 with a particular emphasis on the Arctic aerosol burden. A summary and discussions are proposed in section 5.

2. Data and Method

2.1. POLDER Observations

[5] The POLDER instrument [*Deschamps et al.*, 1994] is a spaceborne radiometer developed by the French national space agency (Centre National d'Etudes Spatiales). National Space Development Agency of Japan (NASDA) has launched two such instruments aboard Advanced Earth Observation Satellite (ADEOS) in 1996 and 2003. Both platforms had a short operating life and the observation archive consists of fifteen months covering the periods from November 1996 to June 1997 (POLDER-1) and from April to October 2003 (POLDER-2). POLDER observes a given target from up to 14 different viewing directions during the satellite overpass, thus providing its reflectance directional signature. Data are acquired in nine different channels from 443 to 910 nm; three of them (443, 670 and 865 nm) with polarization capabilities. The ADEOS satellite was in a Sun-synchronous orbit with a local overpass time of roughly 10:30. The 2200 km swath provides a quasi-global coverage every day, weather permitting. Coverage is minimum at the equator (four observations per 5-day period) and maximum for points located poleward of 37° (several possible observations per day from consecutive orbits). Cloud cover limits the spatial coverage however (clear sky is needed for aerosol retrieval) together with the Sun elevation (high latitude regions are not sampled during the winter months).

[6] The aerosol characteristics are derived separately over land and ocean, using independent algorithms that both generate products with a resolution of about 20 km. The total AOT, the Angström exponent and the accumulation mode AOT are retrieved over the oceans [*Deuzé et al.*, 2000]. The aerosol properties are more difficult to retrieve over land than over oceanic surfaces. Land retrievals are based on polarized light measurements, which limit the information to optical characteristics of the accumulation mode [*Deuzé et al.*, 2001] as coarse particles do not generate significant polarization. Nevertheless, the ability to retrieve the fine mode both over land and oceans makes POLDER particularly suited for studies of anthropogenic aerosols [*Goloub and Arino*, 2000; *Tanré et al.*, 2001]. Other sensors such as MODIS or Multiangle Imaging SpectroRadiometer (MISR) [*Diner et al.*, 1998] for instance also have this capacity and their product could alternatively have been used for the present study.

[7] The POLDER products were used in numerous aerosol studies dealing for instance with the estimate of the aerosol perturbation to the Earth radiative budget [*Boucher and Tanré*, 2000], aerosol and cloud interactions [*Bréon et al.*, 2002], the indirect radiative forcings [*Quaas et al.*, 2004; *Quaas and Boucher*, 2005], and the identification of the aerosol sphericity [*Herman et al.*, 2005]. Previous studies that compared POLDER to TOMS [*Chiapello et al.*, 2000], to MODIS [*Gérard et al.*, 2005], and to other aerosol satellite products [*Myhre et al.*, 2004] over the oceans, have shown their relative consistency.

2.2. LMDz-INCA Model

[8] The LMDz-INCA model refers to the coupling between the Laboratoire de Météorologie Dynamique general circulation model [*Van Leer*, 1977; *Tiedtke*, 1989; *Hourdin and Armengaud*, 1999] and the Interaction with Chemistry and Aerosol model (INCA) [*Hauglustaine et al.*, 2004]. In this study, the atmosphere is discretized on a $3.75° \times 2.5°$ longitude/latitude regular grid with 19 vertical levels. The vertical resolution corresponds to about 400 m in the boundary layer and about 2 km at the tropopause (with 7–9 levels located in the stratosphere). In the present study, the model meteorology is relaxed toward the reanalysis provided by the European Centre for Medium-Range Weather Forecasts (ECMWF) with a relaxation time of 6 hours.

[9] The version of the INCA model used in that work includes a CH_4-NO_x-CO-O_3 chemical scheme representative of the background chemistry of the troposphere. The model transports nine tracers (see Table 1) to simulate major tropospheric aerosol types, including mineral dust, sea salts, sulfates and carbonaceous aerosols (black carbon (BC) and particulate organic matter (POM)). Soluble and insoluble carbonaceous aerosol modes are treated separately. Size distributions for each aerosol type are described using lognormal distributions, which are defined given a variable mass median diameter (mmd) and a constant geometric standard deviation (σ). The AOT is computed from the simulated aerosol mass using the general relationship between the extinction AOT τ and the aerosol mass m [e.g., *Lacis and Mishchenko*, 1994; *Tegen and Lacis*, 1996]:

$$\tau = \frac{3\ qm}{4\rho r_e} \quad (1)$$

Table 1. Parameters Used to Calculate the AOT in the LMDz-INCA Model for Each Aerosol Tracer[a]

Aerosol Type	r_m, μm	r_e, μm	σ_g, μm	Density, kg/m^3	q, m^2/g, 870 nm	ss-alb	Refractive Index at 870 nm
Dust	0.277	0.921	2.00	2650	0.77	0.98	$1.48-0.0009i$
Sea salt	1.185	3.939	2.00	2200	0.22	1.00	$1.48-3\times10^{-6}i$
Sea salt	0.433	1.439	2.00	2200	0.59	1.00	$1.48-3\times10^{-6}i$
Sea salt	0.100	0.171	1.59	2200	0.33	1.00	$1.48-3\times10^{-6}i$
Sulfate	0.100	0.171	1.59	1770	1.78	1.00	$1.52-10^{-7}i$
POM Ins	0.059	0.101	1.59	1500	0.99	0.999	$1.53-0.0001i$
POM Sol	0.100	0.171	1.59	1500	2.35	0.999	$1.53-0.0001i$
BC Ins	0.059	0.101	1.59	1550	4.71	0.47	$1.75-0.43i$
BC Sol	0.100	0.171	1.59	1550	5.18	0.47	$1.75-0.43i$

[a]Modal and effective radii (r_m and r_e), geometric standard deviation (σ_g) in lognormal size distribution, particle density, extinction coefficient (q) at 870 nm, and refractive indices at 870 nm. "Ins" and "Sol" stand for insoluble and soluble, respectively.

where ρ is the particle density, r_e is the effective radius, q is the extinction coefficient. Both τ and q are wavelength-dependent. Table 1 lists the parameters involved in the calculation of the AOT for each tracer. Aerosol size evolution is captured as a function of sedimentation, condensation of sulfuric acid, gas-to-particle formation, ageing of carbonaceous particles and hygroscopic growth [*Gerber*, 1991].

[10] Mineral dust emissions are computed from surface winds; emission factors and threshold wind velocity account for regional characterizations [*Schulz et al.*, 1998; *Claquin*, 1999; *Balkanski et al.*, 2003; *Bauer et al.*, 2004]. Sea salts are emitted in three modes to better account for the wide range of those particle sizes [*Guelle et al.*, 2001; *Schulz et al.*, 2003]. Carbonaceous aerosol emissions are prescribed at a monthly scale following the *Liousse et al.* [1996] inventories. Biomass burning emissions (including agricultural, savannah and tropical forest fires) from the later inventories are modified using satellite-based information to introduce the spatial and interannual variability of fires as observed from space [*Generoso et al.*, 2003]. Sulfate emissions are prescribed on a monthly timescale and closely follow the work of *Boucher et al.* [2002].

2.3. AERONET Ground-Based Measurements

[11] AERONET [*Holben et al.*, 1998] initiated by National Aeronautics and Space Administration (NASA) is a ground-based network, which provides aerosol optical properties. The measurements used in this study are level 2, cloud-screened and quality-assured data [*Smirnov et al.*, 2000]. We used the fine and coarse AOT provided by the spherical particle model almucantar retrievals [*Dubovik and King*, 2000; *Dubovik et al.*, 2000] to estimate uncertainties for both the POLDER and the model fine and coarse AOT. Most AERONET stations were installed after the POLDER-1 era (from November 1996 to June 1997) so that the error statistics are estimated for the POLDER-2 period between April 2003 and October 2003. These statistical errors were then applied to the full assimilation period. We found sixty-five sites with data acquired during the POLDER-2 time period (see section 2.4).

[12] We then used another independent data set from the same network (total AOT from the version 1 direct Sun algorithm) to evaluate the quality of the a posteriori fields. We found sixty sites that acquired a sufficient number of observations for the system evaluation (see section 4.1). Typically, the total uncertainty in AOT (under cloud-free conditions and from newly calibrated instrument) for the direct retrievals is lower than ±0.01 for wavelengths greater than 440 nm (our case) and lower than ±0.02 for shorter wavelengths [*Holben et al.*, 1998]. However, the retrievals of the fine and coarse AOT depend on the bimodal assumption to describe the aerosol size distribution (among other things). According to AERONET definition, particles smaller (larger) than 0.6 microns are in the fine (coarse) mode. Therefore, in some cases (for instance if the real aerosol distribution is close to monomodal distribution) the uncertainties on the fine and coarse AOT could be larger than that of the total AOT.

2.4. Assimilation System

[13] This study relies on Bayesian inference to sequentially combine the observations $\mathbf{y}^o$ (the fine and coarse fractions of the POLDER AOT, AOT_{865}) with the background, or a priori, information $\mathbf{x}^b$ (the corresponding AOT calculated by the LMDz-INCA model). Under the common assumptions of linearity and Gaussian unbiased error statistics, the optimal combination $\mathbf{x}^a$ (the analyzed or a posteriori AOT) at each analysis cycle is given by [e.g., *Rodgers*, 2000]:

$$\mathbf{x}^a = \mathbf{x}^b + \mathbf{K}\left(\mathbf{y}^o - \mathbf{H}\mathbf{x}^b\right) \tag{2}$$

where $\mathbf{H}$ is the observation operator and $\mathbf{K}$ the gain matrix. $\mathbf{H}$ contains the information required to interpolate from the model space to the observation space (hence $\mathbf{H}\mathbf{x}^b$ corresponds to the model results interpolated in the $\mathbf{y}^o$ space; the difference ($\mathbf{y}^o - \mathbf{H}\mathbf{x}^b$) is the innovation vector). In its simplest form, $\mathbf{H}$ corresponds to a geographical interpolation. The innovation vector is weighted by the gain matrix $\mathbf{K}$:

$$\mathbf{K} = \mathbf{B}\mathbf{H}^t\left(\mathbf{H}\mathbf{B}\mathbf{H}^t + \mathbf{R}\right)^{-1} \tag{3}$$

where $\mathbf{B}$ and $\mathbf{R}$ are the a priori and the observational error covariance matrices, respectively. $\mathbf{K}$ is the matrix which produces the best estimate (in the sense of the minimum variance) of the $\mathbf{x}$ vector, given the accuracy of both model and observations.

[14] When the first observation is assimilated, the a priori field $\mathbf{x}^b$ is only based on a free run of the model. After a first assimilation procedure, the model transports the analyzed field ($\mathbf{x}^a$) to the time of the second integration and so on. In

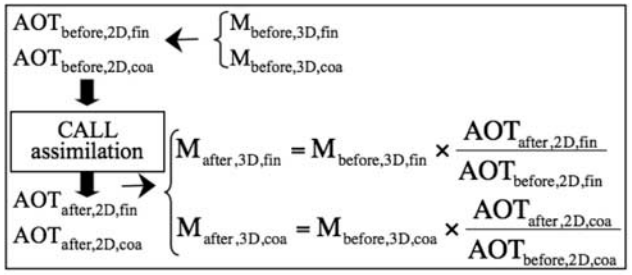

Figure 1. Schematic of the coupling between the assimilation system and the LMDz-INCA model used in this study. "Before" and "after" refer to precall and postcall to the assimilation, respectively. Fine ("fin") and coarse ("coa") fractions of the aerosol are treated separately.

principle, the **B** matrix should evolve in time to account for the added information provided by the satellite data [e.g., *Rodgers*, 2000]. The theoretical temporal variation takes into account the modeling error of the aerosol transport from one cycle to the next. That error in principal could be important in our case, because the representation of some of the processes involved is very uncertain (e.g., deposition and hygroscopic growth). Given the lack of accurate independent observations, the time dependency of the B matrix cannot be usefully estimated and it was therefore neglected in our study. Similarly, spatial and temporal correlations of the errors of the observations and of the background errors were also neglected here.

[15] The LMDz-INCA calculates three-dimensional (3-D) AOT for each aerosol tracer. Simulated AOT can be simply summed in order to retrieve a simulated total column, similar to what is observed by the satellite. Therefore the observation operator **H** is limited to the geographic interpolation from the model to the observation space. In addition, the POLDER products were interpolated onto the model grid. Therefore **H** was reduced to a scalar (H = 1) and the resulting analyzed fields were obtained for each grid cell independently from the neighboring ones.

[16] Figure 1 presents the different steps involved in the computation of the aerosol mass and optical depth following the assimilation procedure in the LMDz-INCA model. The model transports aerosol masses whereas AOT are assimilated. Before calling the assimilation module, column AOT were computed for the fine and coarse modes from the simulated 3-D aerosol mass fields. The assimilation of POLDER then provided an a posteriori AOT estimate for each mode. These AOT were then turned back into 3-D aerosol mass fields for each tracer using the relative contribution and vertical profile of the a priori fields. During the 6-hour integration time, POLDER observations are distributed over a quarter of the Earth. Typically, there are between 2500 and 3000 daily observations for the fine mode and between 1500 and 2000 for the coarse mode (after the observations were mapped onto the model grid).

[17] The variances of the model and of the observation errors determine the balance between the two sources of information in the assimilation process. Independent measurements from the AERONET networks (see section 2.3) were chosen to consistently define weights to be given to the a priori and to the observations. However, a major difficulty lies in the definition of errors for each model grid box as only a limited number of AERONET stations (65), irregularly distributed over the Earth, were available. We divided the world into ten regions that are homogeneous to the first order in terms of aerosol type and/or process, including eight continental regions (mainly corresponding to different emission types) and two oceanic areas (Figure 2). A criterion based on the distance between ocean boxes to continents was applied to distinguish between regions under the strong influence of sources (for instance North Atlantic) and remote regions (for instance South Pacific). AERONET measurements were sampled to keep only those corresponding to the satellite overpass. To be consistent with the 6-hour integration time step, measurements in stations located in the easternmost quarter of the globe were kept if they were acquired between 0 h and 6 h UT, in the second quarter only if they were acquired between 6 h and 12 h and so on. POLDER observations (regridded onto the model grid consistently with the data being assimilated) and model outputs were then compared to the AERONET 6-hour-mean values. We assumed that all model grid boxes within a given region have similar statistical errors.

[18] The model errors (model minus AERONET) and the observation errors (POLDER minus AERONET) were computed as standard deviations for each region and for each mode. In the rest of the manuscript, we therefore refer to those quantities as (model or observation) error standard deviation. A validation exercise against AERONET measurements (not shown) indicated that the errors in the satellite estimates of coarse and fine mode AOT are weakly correlated (less than 0.36). As a consequence, these correlations were neglected in our assimilation system. Two estimates of error standard deviation were made either considering all Sun photometer measurements available for each region or after grouping them into AOT bins. The second estimate yields an error that is a function of the AOT values, as one

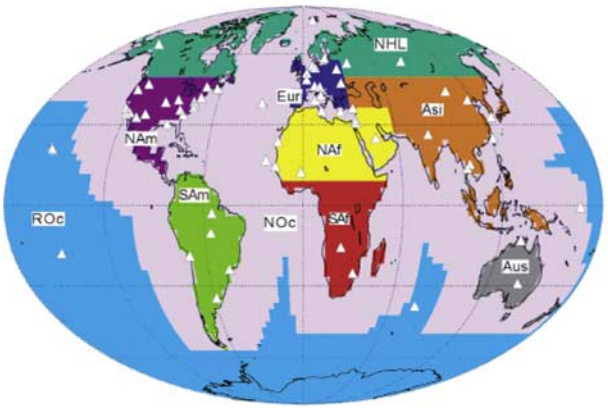

Figure 2. Map of the ten regions selected for the estimation of model and observation errors. The triangles correspond to the sixty-five AERONET stations used to estimate both the model and the observation errors. NAf, North Africa; SAf, South Africa; NAm, North America; SAm, South America; Eur, Europe; Asi, Asia; NHL, northern high latitudes; Aus, Australia; NOc, "near-ocean"; ROc, "remote-ocean."

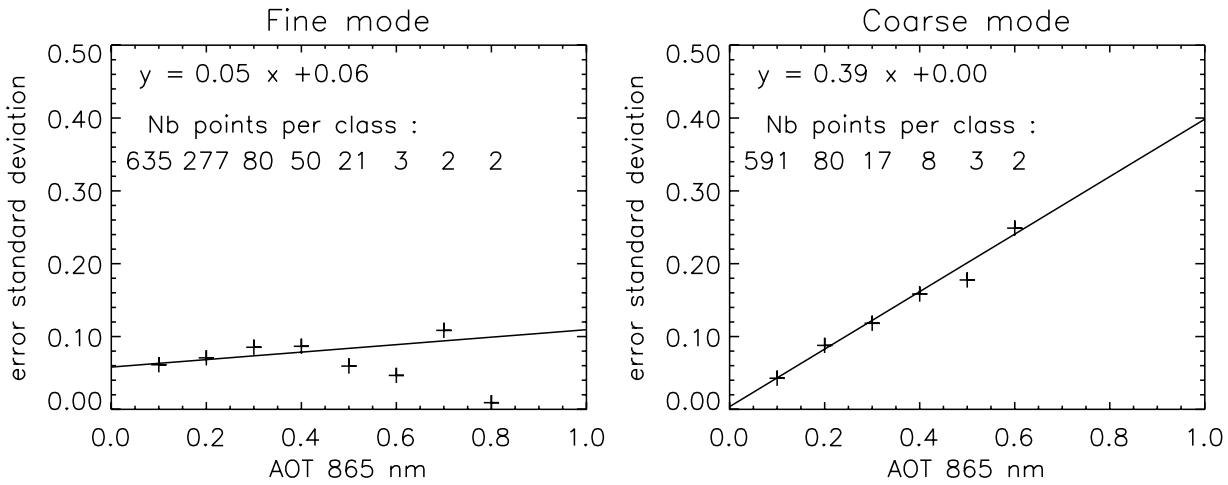

Figure 3. Model error standard deviation as a function of the AOT for the region "near-ocean" (NOc) for the (left) fine and (right) coarse mode. The line is a best fit through the data points.

may expect the model and observation errors to be smaller, in absolute, when the AOT is smaller. Some regions showed a clear dependency of the error with the AOT, as illustrated in Figure 3. In such case, one may estimate the error on both model and satellite observations as $\sigma = a\tau + b$ where τ is the observed or simulated AOT. This estimate was chosen if σ was defined at least on a three-bin basis, each bin being kept if more than 15 data were found. Some regions did not show such clear trend, mostly for lack of data for the largest AOT, in which case the retained error was simply a constant equal to the standard error over the whole data set. Results for each region and each mode are presented in Table 2.

[19] In the fine mode, the largest error standard deviations are obtained in the densely populated and industrialized regions of Asia and Europe as well as in regions with biomass burning such as South Africa. The assimilation system will thus attribute a lower weight to the model compared to the observations in these regions (Table 2), which appear to be reasonable in view of the current representation of certain processes in the model (e.g., biomass burning sources, deposition). In oceanic regions, larger standard deviations are found over the "coastal" pixels than over the open oceans. This is also expected as grid points close to the coasts are under the influence of localized sources whose spatial and temporal distributions are not accurate in the model. On the other hand, some results derived from the comparison of POLDER to AERONET are somewhat unexpected. In particular, we found larger errors for Asia than for North America and Europe, even though there is no obvious reason for those three regions to be "seen" differently by POLDER. This may result from the relatively small number of AERONET sites in Asia, and may indicate that the statistics are not fully representative for that region.

[20] Coarse mode data are limited to the oceans. The error estimate is based on coastal or island stations, which decrease considerably the amount of available data, and few are representative of the open oceans.

[21] The formalism of data assimilation as described in equations (2) and (3) applies to unbiased variables. Hence differences between observations and simulated values should be null so that only random errors are corrected. Model and observations biases to AERONET data are estimated in parallel to the error standard deviations, using the same data set in each region and for each mode. Results are of the same order of magnitude as the error standard deviations, which implies that the bias should be taken into account. For convenience, the sum of the model bias and of the POLDER

Table 2. Error Standard Deviation for the Model (σ_M) and POLDER (σ_P), Estimated by Comparisons to AERONET Measurements in Each Region[a]

	Fine Mode			Coarse Mode		
Region	σ_M	σ_P	N	σ_M	σ_P	N
NAf	0.033	0.044	252	NPO	NPO	NPO
SAf	0.063	$0.214\tau + 0.01$	502	NPO	NPO	NPO
Nam	$0.179\tau + 0.033$	0.050	1253	NPO	NPO	NPO
Sam*	0.063	$0.214\tau + 0.01$	137	NPO	NPO	NPO
Eur	$0.023\tau + 0.102$	0.048	846	NPO	NPO	NPO
Asi	$0.335\tau + 0.180$	$0.45\tau + 0.064$	243	NPO	NPO	NPO
NHL*	$0.179\tau + 0.033$	0.050	90	NPO	NPO	NPO
Aus	0.012	0.012	184	NPO	NPO	NPO
NOc	$0.051\tau + 0.058$	$0.277\tau + 0.015$	739	$0.395\tau + 0.004$	$0.287\tau + 0.01$	611
ROc	0.012	0.014	196	0.015	0.035	194

[a]Estimates are based on N measurements, indicated in the right columns. Statistics for regions followed with asterisks are chosen equal to those of similar regions in terms of aerosol processes. Region labels are given in the caption of Figure 2. NPO indicates no POLDER observations in that mode over continents.

Table 3. Error of the Analyzed Fields[a] (e_A) Averaged per Region[b] and Over the Assimilation Period

Region	Fine Mode	Coarse Mode
NAf	0.028	NPO
SAf	0.027	NPO
Nam	0.032	NPO
Sam	0.020	NPO
Eur	0.044	NPO
Asi	0.077	NPO
NHL	0.035	NPO
Aus	0.012	NPO
NOc	0.024	0.024
ROc	0.010	0.018

[a]Square root of the mean values of A (equation (4)).
[b]Region labels are given in the caption of Figure 2. NPO indicates no POLDER observations in that mode over continents.

bias (averaged per region and for the POLDER-2 period) is removed from the POLDER observations in each region.

3. A Posteriori Validation

[22] Different diagnostics exist to quantitatively evaluate an assimilation algorithm [*Talagrand*, 2002]. In this section we discuss the theoretical error, stability, consistency and optimality of the assimilation system.

[23] The error of the analyzed fields depends on both a priori and observation errors. The theoretical expression of the analysis error is given by [e.g., *Rodgers*, 2000]:

$$\mathbf{A} = \mathbf{B} - \mathbf{B}\mathbf{H}^t(\mathbf{H}\mathbf{B}\mathbf{H}^t + \mathbf{R})^{-1}\mathbf{H}\mathbf{B} \tag{4}$$

[24] We apply this relationship to our system and present results averaged per region and for the POLDER-2 period in Table 3. By construction, the analysis error should be smaller than both the model and observation errors as seen in Tables 2 and 3.

[25] One of the criteria used to verify the stability of the assimilation system is to plot the temporal evolution of the innovation vector, called **d** hereinafter. Its expression is given by:

$$\mathbf{d} = \mathbf{y} - \mathbf{H}\mathbf{x}^{\mathrm{b}} \tag{5}$$

and corresponds to the deviation between the observations and the a priori fields. Figure 4 presents the monthly mean variations of **d** during the POLDER-2 period. We also indicate the standard deviation of the daily global mean innovation vector (as error bars on the plot), in order to show the daily variability of the results. For the fine mode assimilation system, the monthly mean is nearly zero, which was expected as the biases were removed from the assimilation system. More importantly, there are no significant temporal variations of **d** and the standard deviations are small compared to the monthly mean values. On the other hand, for the coarse mode, the system presents oscillations of the **d** values around 0.03, which indicates that some bias remain in the system. We can here question the significance of the bias in the coarse mode since the assimilation for this mode occurs only over oceanic regions whereas the error statistics are derived from the closest continental regions (coasts and islands), which are unlikely to be representative of the whole oceanic regions.

[26] In order to evaluate the consistency of the assimilation system, we use a simple diagnostic, which is provided by the following quantity:

$$c = E\left(\frac{1}{2}d^t[\mathbf{H}\mathbf{B}\mathbf{H}^t + R]^{-1}d\right) \tag{6}$$

here E is the expectancy function. For a perfectly consistent system, c is close to p/2, with p the number of observations. In our case, p = 1 since we solved the Bayesian problem in a scalar form. The results are c = 0.25 and c = 0.93 for the fine and coarse mode, respectively. Those values correspond to the global average for the POLDER-2 period. Many authors have used this criterion to evaluate the consistency of their assimilation system. A general conclusion is that *c* is often smaller than the expected values, typically with a factor from 1/2 to 2/3 [*Talagrand*, 2002]. For the fine mode assimilation system, *c* is smaller than p/2 within a factor 1/2. This means that the matrix [$\mathbf{H}\mathbf{B}\mathbf{H}^{\mathrm{t}}$ + **R**] is larger than it should be. This result has the same order of magnitude and sign as those of other studies cited by *Talagrand* [2002], who explains that this difference could be due to an overestimate of the error covariance matrix of the a priori, **B**. In the present study, the a priori and observation errors (**B** and **R)** were derived using the same method and data set. However, the a priori error (i.e., **B**) was based on the free model outputs, while, the a priori field includes some information from the observations (after the first time step). Thus our estimated a priori error is probably overestimated, which may explain the underestimate of the *c* parameter. For the coarse mode system, *c* is larger than p/2. For the same reasons, this result indicates that **B** + **R** is underestimated. Moreover in absolute, the result is worse than in the fine mode assimilation, which points to a worse definition for **B** and **R**. This result could be explained by a lack of representational measurements in the oceanic regions. The consistency of the assimilation system is closely dependent on the input error covariances [*Ménard et al.*, 2000]. Therefore our assumption to consider fine and coarse products as two independent states (i.e., not correlated) may also impact the results presented here.

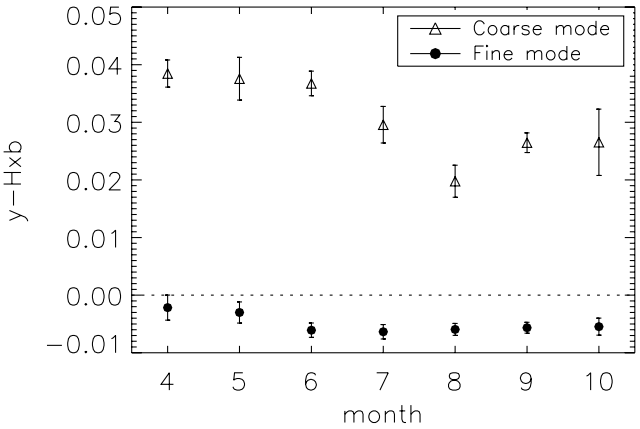

Figure 4. Mean and standard deviation of the daily global innovation vector as a function of the month for the period from April to October 2003 for the (top) coarse and (bottom) fine mode products.

Table 4. Results for the Optimality Test (Equation (7))

	Fine Mode	Coarse Mode
$E(x-x^a)$	10^{-3}	-4×10^{-3}
$E[(x-x^a)d^t]$	5×10^{-4}	-2×10^{-5}

[27] The notion of optimality means that the combination of the a priori and the observations is done in the sense of minimum of variance. Verifying the optimality of the system is equivalent to verifying the two following criteria:

$$E(x - x_a) = 0$$
$$E[(x - x_a)d^t] = 0 \quad (7)$$

here x is an independent observation of the state (i.e., not used in the assimilation system), d the innovation vector. We apply these criteria to our system using the AERONET data as real state. Table 4 presents the estimate of the left terms of equations (7). Values are small in comparisons of the estimate of error standard deviations, so that we can consider that the assimilation system provides results that are fairly optimal, despite the above-mentioned lack of consistency.

4. Results

4.1. Global Aerosol Distribution

[28] We performed comparisons between the global fields obtained from the assimilation procedure (a posteriori) and from the standard model (a priori). Figures 5 and 6 present the differences between the a posteriori and a priori aerosol fields that will be referred as "increment" in the rest of the text, for the coarse and fine mode, respectively.

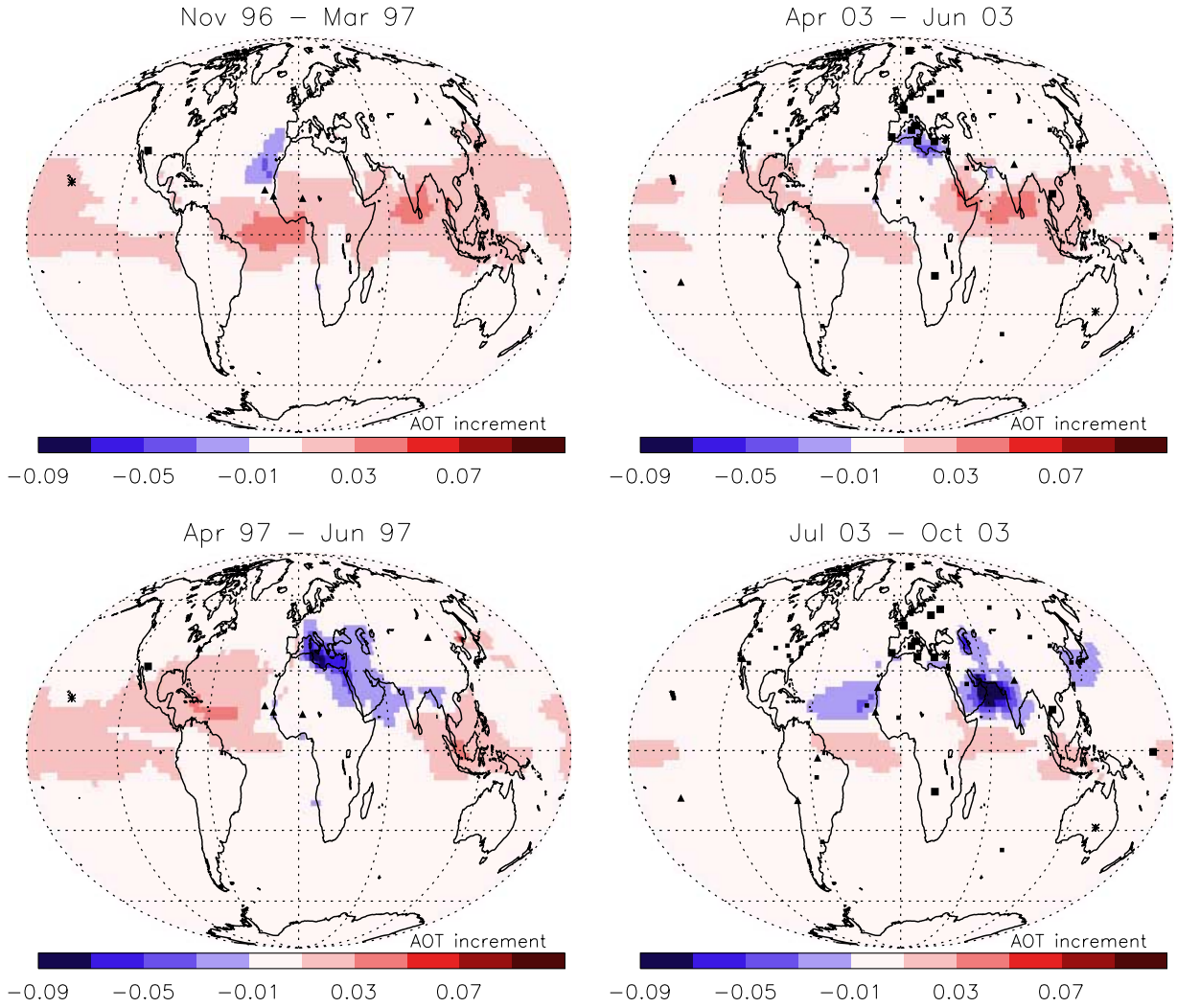

Figure 5. Difference between the a posteriori and a priori fields for the coarse mode ("increment"). AOT increment at 865 nm are averaged for the periods (top left) November 1996 to March 1997, April–June (bottom left) 1997 and (top right) 2003, and (bottom right) July–October 2003. The symbols correspond to AERONET stations used for the validation. The squares locate the stations where the assimilation leads to a reduction of the RMS errors (computed from the daily data) compared to AERONET (small squares indicate reduction between 5 and 25%, and large squares indicate greater than 25%). The triangles indicate the stations with no significant changes (difference in the RMS errors lower than 5%). The stars indicate the stations with an increase of the RMS errors with the assimilation.

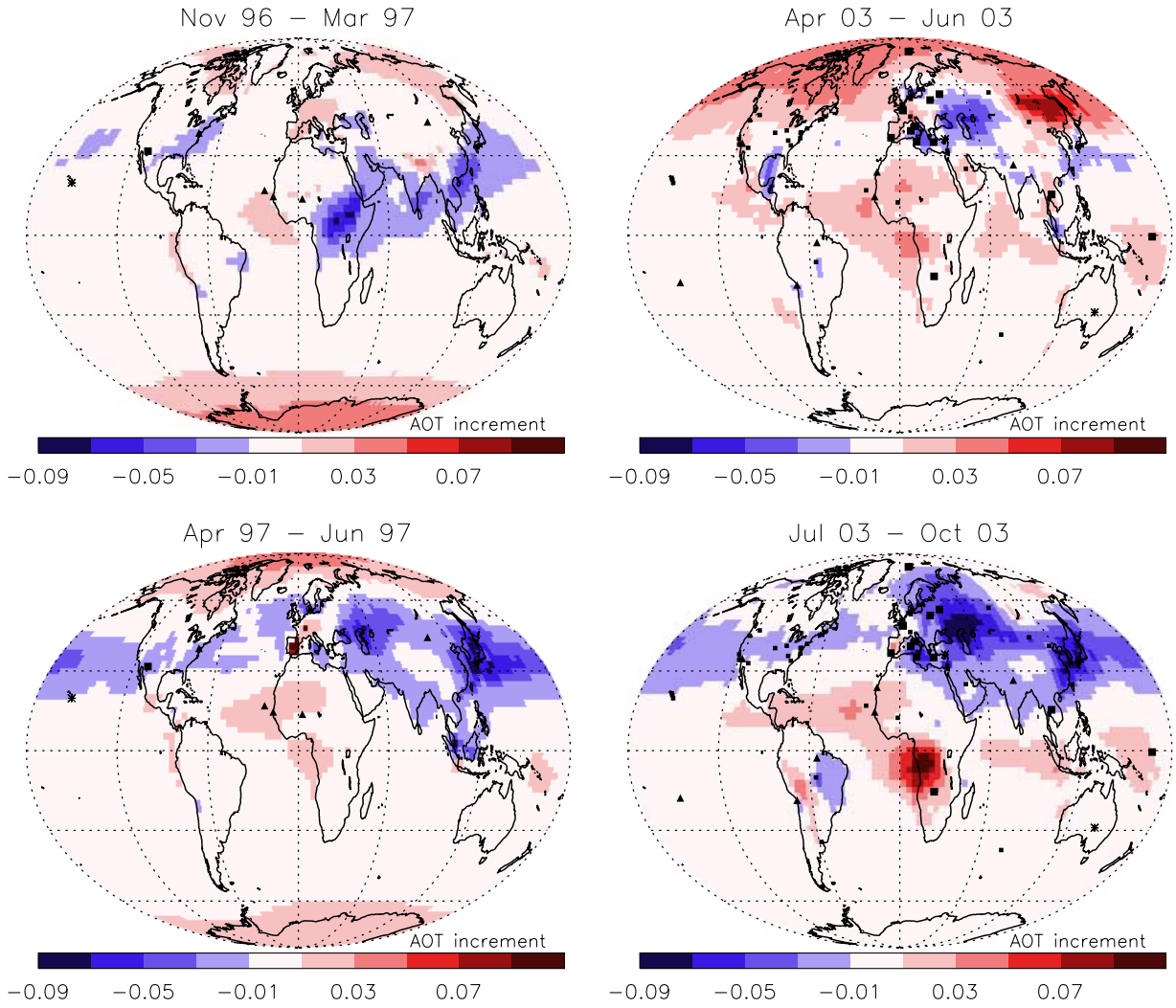

Figure 6. Same as Figure 5 for the fine mode.

Fifteen months were covered in total: from November 1996 to June 1997 (POLDER-1) and from April to October 2003 (POLDER-2), which allow to examine a complete annual cycle and the interannual variability for the three common months. Thus we analyzed the results considering three periods: (1) from November to March (1997), (2) from April to June (1997 and 2003), and (3) from July to October (2003).

[29] For the coarse mode (dust and sea salts) (Figure 5), there are no significant modifications over land since POLDER observations are not available. Over the oceans, the largest increments are located in the tropical and temperate latitudes. There is a tendency for the model to overestimate the AOT (compared to POLDER) in the regions near the Saharan dust sources (North Atlantic; Mediterranean Sea in April–June), which may be due to an overestimate of the dust sources in that region. In contrast, the model underestimates the AOT in the remote (from dust sources) oceanic regions. For instance, in November–March (as well as in July–October but to a lower extent), the simulated AOT are corrected for an excess off the coasts of Mauritania, downwind of Saharan dust source, whereas they are corrected for a deficit in the dust continental outflow in the Caribbean Sea and the Gulf of Guinea. This is consistent with the discrepancies found between the model results and different satellite products (POLDER and TOMS) as this was shown in this region with the analysis of daily aerosol fields during a large aerosol event in March 1997 [*Generoso*, 2004, see chap. 4, Figure 4.5]. These may indicate a possible misrepresentation in the model of processes occurring during aerosol transport (e.g., advection, deposition, hygroscopic growth or ageing of the particles during transport).

[30] In the fine mode (sulfates, carbonaceous aerosols and fine sea salts), the increments are larger in amplitude and extent to larger regions than for the coarse mode (Figure 6) since both land and ocean data are assimilated. Although there is a large interannual variability in the April–June period, we note some persistent patterns. First, the model overestimates the AOT (compared to POLDER) in the urban and industrial regions of the Northern Hemisphere, in particular in Eurasia, Asia and the Mediterranean Sea. This is true also in July–October 2003. A large part of this signal is explained by the presence of sulfate aerosols in the model. Another persistent pattern is a strong underestimate of the model AOT in the biomass burning regions of Siberia (April–June 2003) and South Africa (July–October 2003).

One likely explanation is an underestimate of the biomass burning aerosol sources. In particular, [*Nedelec et al.*, 2005] reported particularly high carbon monoxide concentrations in the atmosphere during the summer of 2003 due to natural fires that occurred in the Lake Baïkal region. Finally, over the Sahara, the a posteriori fields show enhanced fine AOT composed of sulfates and carbonaceous aerosols although no sources of such aerosol types are present there. The POLDER retrieval indicates the presence of fine aerosols together with the dominant coarse particles (which are likely to be dust). Dust are only described in the coarse mode in the model, so that the assimilation process distributes the increment of the fine mode to other species, even though they are present in small amount in the a priori model fields. This points out to a limitation of the method.

[31] On the maps presented in Figures 5 and 6, we also plotted the position of all the AERONET stations where a sufficient number of data allows an evaluation of the assimilated field quality (using total AOT measurements, see section 2.3). The size of the symbols (squares) depicts the improvement between the two versions of the model as diagnosed by the root-mean-square errors (RMS) of the a priori and a posteriori daily fields (compared to AERONET).

[32] During the POLDER-1 time period, only Sun photometer stations over the Sahara acquired a sufficient number of observations for the system evaluation. As the stations are located in the dust source regions, no significant differences are observed between the two versions of the model since no observations of the coarse mode were assimilated over land. During the POLDER-2 period, a larger number of ground-based measurements is available. Over the Mediterranean Sea, where we observed large differences between the a priori and a posteriori both in the fine and coarse mode distributions, all the available AERONET stations show improvements. The example of Oristano (Italy) is presented in Figure 7. The improvement is significant both in terms of mean value and seasonal cycle. The reduction in the total AOT is mainly due to the reduction of the fine mode AOT (not shown), which is particularly overestimated by the free model. A similar feature is observed for the other Mediterranean sites (Lampedusa, Roma, Nes Ziona, El Arenosillo). The reduction of the error both in terms of mean and standard deviation is in particular significant for late spring and summer (May, June and August) (Figure 7). Similarly, the consistency with AERONET measurements is improved over all stations in Eurasia (Figures 5 and 6), in particular for the mean aerosol load (one example over the Moscow area is shown in Figure 7). The improvement is not as clear neither in stations over northern Europe (Helgoland, Gotland, Hamburg), where the strong high bias (not shown) in comparison to AERONET is only slightly reduced, or over northeast America where no significant changes are seen.

[33] The POLDER-2 observation period covers the biomass burning seasons over South America and South Africa, but few Sun photometer data are available for comparison. The results over Mongu in Africa are shown in Figure 7. The timing of the burning season is well reproduced by both the a priori and the a posteriori fields. The amplitude of the annual cycle remains underestimated in the a posteriori, although the assimilation yields improvements. The results of the a priori in Alta Floresta in South America (not shown) present similar patterns than in South Africa, but no significant differences are found with the a posteriori.

[34] Very few AERONET sites are available during the POLDER era over Asia and Figure 7 shows the results over Gosan in South Korea. The a priori field presents a large overestimate of AOT during the summer months (June to August), which is successfully corrected with the assimilation. On the other hand, we note that the AOT is largely underestimated both in the a priori and a posteriori for April and May. The Gosan site is located in the Che-Ju Island in South Korea, downwind of the Asian continent. Large dust outbreaks occur frequently in eastern Asia in spring and can be transported toward South Korea, which result in enhanced aerosol load in the Che-Ju Island [*Carmichael et al.*, 1997; *Chen et al.*, 1997; *Chun et al.*, 2001; *Chuang et al.*, 2003]. It is likely that the high aerosol load in Gosan in spring 2003 reflects such dust episodes. In that case, the assimilation system is not able to correct the a priori model underestimate since no POLDER observations of coarse particles have been assimilated over land.

4.2. Implications for the Arctic Aerosol Burden

[35] Climate modeling and recent observations indicate that the Arctic region is strongly affected by climate change. Although there are no significant local sources, the Arctic atmosphere presents high concentration of aerosols, mostly fine particles resulting from the long-range transport of pollution from urban and industrial regions as well as from biomass burning [e.g., *Shaw*, 1995; *Koch and Hansen*, 2005]. The so-called ''Arctic haze'' phenomenon occurs mostly during the winter-spring period, when the polar vortex weakens and allows greater exchange between air masses from low and polar latitudes. Moreover, during winter months, the Arctic climate is characterized by small amounts of clouds and precipitation, thus weak deposition of aerosols, which contributes to their accumulation in the atmosphere. *Clarke and Noone* [1985] show that BC reduces the snow absorption with a strong impact on the surface albedo and evaporation rate. *Rinke et al.* [2004] recently showed that via the direct aerosol effect, aerosols may modify the regional circulation patterns and the hydrological cycle in the Arctic. However, Arctic haze studies still suffer from a lack of regional and continuous aerosol monitoring, which could be provided with satellites. Unfortunately, current satellite observations cannot be used to retrieve tropospheric aerosol load over snow- or ice-covered surfaces. In this context, a combination of satellite observations over high latitude, atmospheric transport modeling and assimilation techniques may fill a gap and provide the needed information to document the Arctic aerosol load. In the rest of this section, we present a first attempt in this direction.

[36] Figure 8 presents the increment (differences between the a posteriori aerosol fields and the a priori), centered over the North Pole, for the overlap period of the two POLDER mission: from April to June 1997 and 2003. Figure 8 shows also POLDER aerosol estimates from April to May 2003. Grey areas correspond to regions where no successful retrieval is available during the month, either because the Sun is too low over the horizon or because of the presence of cloud or ice-snow-covered surface. The increments on

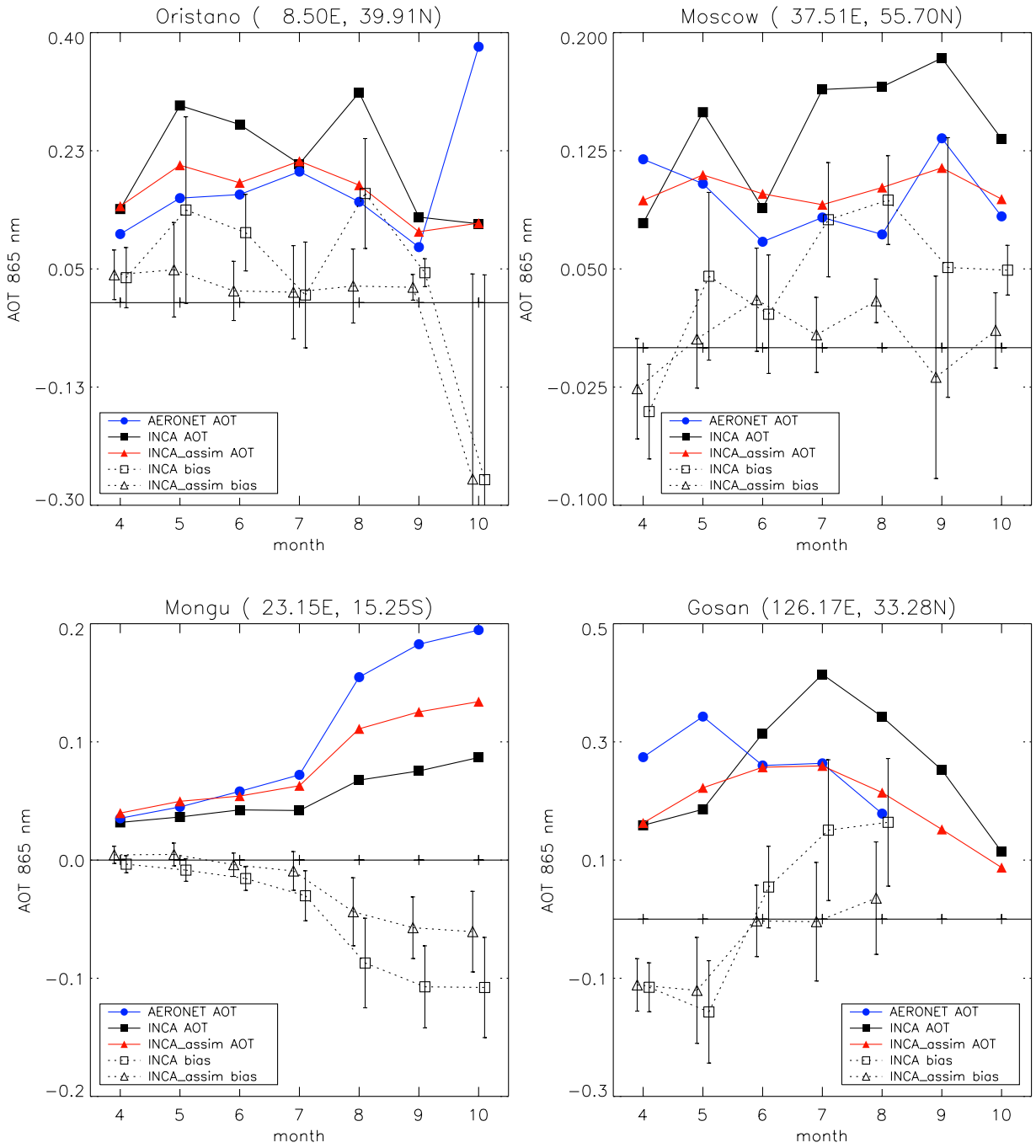

Figure 7. Monthly mean total AOT at 865 nm simulated with ("INCA_assim") and without ("INCA") assimilation and measured at AERONET stations (solid lines and solid symbols). Dotted lines and open symbols represent the mean and standard deviation (error bars) of the differences between the two versions of the model and individual AERONET measurements (model minus measurements).

the AOT_{865} during this period are between 0.01 and 0.07. Different studies reported background values of 0.06 at 500 nm and defined an Arctic haze event to occur when the AOT_{500} is greater than 0.1 [e.g., *Herber et al.*, 2002; *Yamanouchi et al.*, 2005]. For the fine particles that are likely to be dominant in the Arctic region, an Angström coefficient equal or greater than 1 is expected [*Herber et al.*, 2002] so that the ratio between the AOT_{500} and AOT_{865} is on the order of 2. As a consequence, the assimilation increments have the same order of magnitude as the background AOT generally measured there.

[37] Since there are no POLDER observations available over the Arctic, the increments in that region result from the transport of aerosol loads constrained by POLDER over distant regions. In May and June, the assimilation results in a much larger increase of AOT in 2003 than in 1997 (Figure 8). AOT increased possibly as a consequence of the large anomalous biomass burning that occurred in

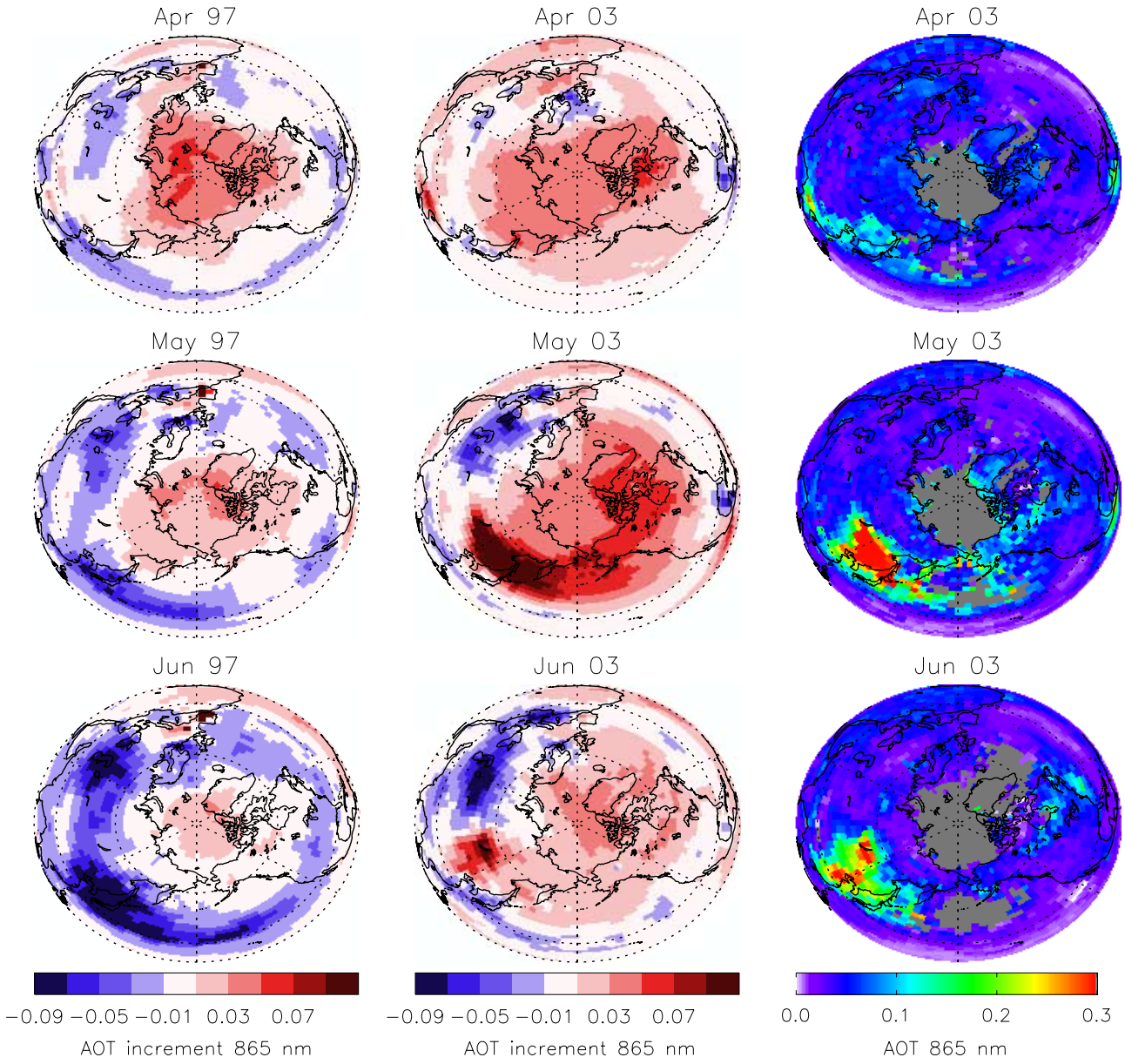

Figure 8. Monthly mean difference between the a posteriori and a priori fine AOT at 865 nm for the April–June period (left) 1997 and (middle) 2003, with a projection centered over the North Pole. (right) The POLDER fine AOT at 865 nm are also presented with the same projection and for the same months.

Russia during summer 2003 (from May to August) [*Jaffe et al.*, 2004; *Bertschi and Jaffe*, 2005], which are mainly located in the source region around Lake Baïkal in May and June. POLDER captures the AOT resulting from the smoke plumes in this region, which result in the large positive increments observed. *Damoah et al.* [2004] investigated the transport of smoke from the Russian fires from 10 to 31 May 2003 and showed that the smoke plumes were transported from the Russian area to Alaska via the Bearing Sea, crossed to eastern Canada and then proceeded across the Atlantic to Europe on their way back to Russia. The monthly mean increments in May 2003 in the regions downwind the Asian continent and circumpolar are consistent with the long-range transport described by *Damoah et al.* [2004]. In addition, they indicate that the plume could have reached Arctic latitudes. This is also consistent with the recent results of *Koch and Hansen* [2005], who used a global model to point out the role of Asian biomass burning north of 40°N in the BC load over Arctic.

[38] AERONET surface measurements of AOT over the Arctic for this period are only found in Longyearbyen, located 15°E, 78°N, in the Spitsbergen. Figure 9 presents the comparisons between AERONET total AOT_{870} and that derived from the a priori and a posteriori model. Longyearbyen independent measurements (i.e., not used in the assimilation system) show the winter-spring Arctic haze aerosol load and rather low values in September, which are in contradiction with the LMDz-INCA model results. The simulated peak in September–October is explained mostly by sulfates (not shown), which could indicate that sulfate

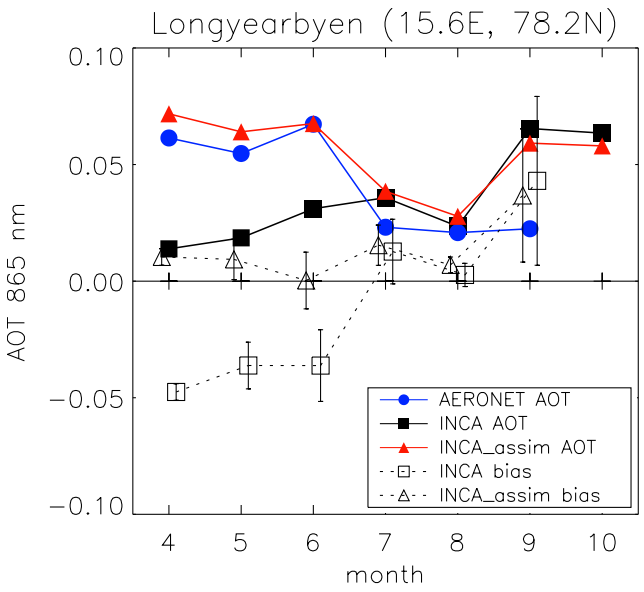

Figure 9. Monthly mean total AOT at 865 nm simulated with ("INCA_assim") and without ("INCA") assimilation and measured in Longyearbyen in 2003 (AERONET), within the Arctic Circle (solid lines and solid symbols). Dotted lines and open symbols represent the mean and standard deviation (error bars) of the differences between the two versions of the model and individual AERONET measurements (model minus measurements).

sources are overestimated in the urban and industrial regions of the northern midlatitudes (consistent with our findings in Figure 6 for the July–October period). This discrepancy remains after assimilation, although it decreases slightly during September and October. One possible explanation is that, if the northern sources are overestimated in the model and are not or only partially corrected with the assimilation of satellite data, then the excess of mass can be transported to the Pole, where no POLDER observations are available to constrain the Arctic aerosol load. Nonetheless, the assimilated AOT matches the AERONET measurements well for the spring period. The increase in total AOT in the simulation is caused by the increase of sulfates and carbonaceous aerosols. Note that indications of the relative abundance of sulfates, BC and OC cannot be provided by the assimilation system, since there is no information relative to speciation available from the satellites.

[39] *Herber et al.* [2002] documented the aerosol load continuously between 1991 and 1999 based on Sun photometer measurements in the Spitsbergen and found that the seasonal maximum occurs in spring (March–May) while the lowest AOT are measured in fall and winter. They also reported that this seasonal variation was observed over the whole Arctic, with the highest values occurring always in spring. Figure 10 presents the monthly mean AOT of the fine particles, averaged for the latitudes north of 75°N, from our standard model and the a posteriori fields. The standard simulation shows seasonal variations that are in contradiction with those typically observed in the Arctic. First, there are no clear variations for 1996–1997 with a difference of 0.01 between the lowest simulated AOT (December) and the highest (November and January), whereas *Herber et al.* [2002] reported a difference of about 0.05 between the lowest fall values and the highest spring ones based on AOT averaged over the period 1995–1999. Then, the standard model presents higher AOT values for summer and fall than for spring in 2003. On the other hand, the a posteriori AOT present a seasonal cycle, which is characteristic of the observed aerosol load in Arctic both for the 1996–1997 and the 2003 period. In 1996–1997, the amplitude of the seasonal variations is 0.047 with the maximum value in April (0.06). This is in good agreement with the measurements reported by *Herber et al.* [2002] for the spring "Arctic haze" mean values (about 0.08, while they reported spring background values of about 0.04). In 2003, the amplitude of the variations is 0.039 between the highest value simulated in May and the lowest one in October. Interestingly, the a posteriori fields present the maximum AOT in May and June 2003, which can suggest the impact of the Russian fires. The assimilation of POLDER data increases the maximum AOT by a factor three both in 1997 and 2003.

5. Summary and Discussion

[40] In this study, we applied the data assimilation technique to provide improved global aerosol distributions. POLDER fine and coarse AOT were assimilated separately into the global 3-D atmospheric chemistry and transport model LMDz-INCA for two periods from November 1996 to June 1997 and from April to October 2003. The error statistics of the model and of the observations, which strongly constrain the a posteriori fields, were estimated on a regional basis using more than sixty ground-based sites. However, independent data are missing to validate the coarse mode assimilation. In contrast, for the assimilation of the fine mode products, validation data are available for all continents in 2003. Despite the scarcity of the measurements, reduction of root-mean-square errors are found in

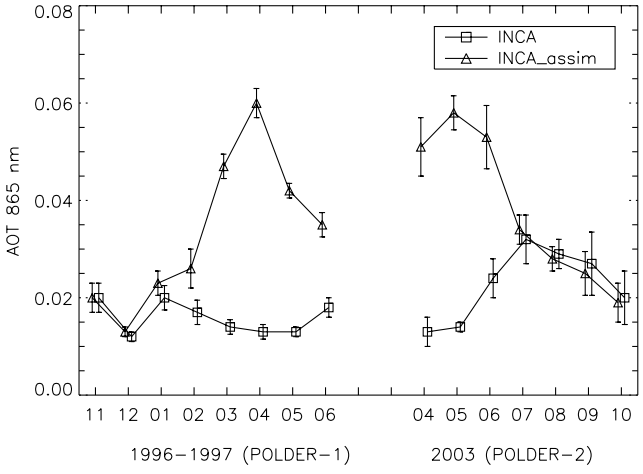

Figure 10. Monthly mean and standard deviation of the daily simulated AOT of the fine particles, averaged for the latitudes north of 75°N, from the standard ("INCA") and the a posteriori ("INCA_assim") fields for the two POLDER periods, from November 1996 to June 1997 (POLDER-1) and from April to October 2003 (POLDER-2).

most regions, with the largest reductions found in the Mediterranean Sea and Eurasia, when the a posteriori fields are compared to an AERONET independent data set.

[41] The use of the assimilation technique in the context of global atmospheric modeling provides continuous aerosol fields, which are of particular interest in the regions where current satellite observations cannot be used to retrieve the aerosol load. In this study, we particularly emphasize implications for the Arctic aerosol burden since the presence of snow- or ice-covered surfaces prevents continuous monitoring of the aerosol load. The a posteriori fields show a noticeable improvement with regards to the seasonal variations of the Arctic aerosol load. AERONET measurements in the Spitsbergen in 2003 that show a spring peak in AOT, which is typically associated with the Arctic haze, are fairly well reproduced by the a posteriori fields. The results suggest also that the large biomass burning events that occurred in spring 2003 in Russia are likely to contribute significantly to the Arctic aerosol load in May and June 2003. The assimilation system allowed us to successfully reproduce the Arctic seasonal variations, which is an encouraging result. Since no POLDER observations are available over the Arctic, this agreement is an additional indication that the winter-spring Arctic peak results mostly from the transport of aerosol from the mid northern latitude sources.

[42] Although the application of the assimilation technique to the issue of global aerosol distribution show encouraging results in this study, some large sources of uncertainties remain. First, questions regarding the vertical distributions of aerosol were not discussed here since satellite observations do not provide yet the valuable information needed to constrain, or at least evaluate, the models on a global scale. *Guibert et al.* [2005] evaluates the ability of the LMDz-INCA model to reproduce aerosol extinction vertical profiles observed with seven lidars from the European Aerosol Research Lidar Network (EARLINET). Their results show that the model succeeds to reproduce the mean annual aerosol vertical distribution over European sites. On the other hand comparisons based on individual profiles show moderate correlation between model and data. This points out to a large uncertainty in the modeling of aerosol daily distributions. The Cloud and Aerosol Lidar Pathfinder Satellite Observations (CALIPSO) mission, launched in 2006, will provide a unique data set of aerosol vertical profiles on a global scale, which will offer undoubtedly a valuable piece of information either to evaluate or to constrain the aerosol model using, for instance, assimilation techniques. In addition, the so-called A-train, a constellation of satellites flying in formation around the globe provides near simultaneous measurements of different atmospheric constituents and parameters including aerosol load information acquired by MODIS and PARASOL (a radiometer similar to POLDER) together with the CALIPSO lidar. In some sense, the observations provided by these sensors are complementary and can provide large constrains in an assimilation procedure such as the one proposed in this paper, to improve our understanding of the daily aerosol variability.

[43] Another source of uncertainties in the aerosol modeling is the relative abundance of one species in comparison to the others. Despite our effort to constrain the simulated coarse and fine aerosol fraction, the distribution per species within each mode is kept unchanged. One step further in this direction could be to use the notion of anthropogenic versus natural AOT as derived from MODIS observations by *Kaufman et al.* [2005]. This information can help to improve our understanding of the natural versus human-induced aerosol effect.

[44] Finally, the Kalman filtering method as used in this study shows encouraging results in terms of reduction of uncertainties in aerosol distributions. However, this method does not modify the representation of processes involved in aerosol modeling (e.g., representation of emissions, deposition, hygroscopic growth). *Hakami et al.* [2005] have recently applied adjoint inverse modeling in the framework of the Asian Pacific Regional Aerosol Characterization Experiment (ACE-Asia) in order to optimally recover anthropogenic and biomass burning emissions of black carbon. Those techniques would be remarkably suited to constrain aerosol surface fluxes at a global scale in order to take into account their high spatial and temporal variability.

[45] **Acknowledgments.** The satellite data come from the POLDER instrument developed by the Centre National d'Etudes Spatiales on board the ADEOS platform developed by NASDA. The authors gratefully acknowledge the AERONET principal investigators and their staff for establishing and maintaining the 69 sites used in this investigation. We thank Christiane Textor, Sarah Guibert, Olivier Boucher and Didier Hauglustaine, who considerably contributed to the development of the model version used in this study.

References

Balkanski, Y., M. Schulz, T. Claquin, C. Moulin, and P. Ginoux (2003), Global emisisons of mineral aerosol: Formulation and validation using satellite imagery, in *Emission of Atmospheric Trace Compounds*, edited by C. Granier, P. Artaxo, and C. E. Reeves, pp. 253–282, Springer, New York.

Bauer, S. E., Y. Balkanski, M. Schulz, D. A. Hauglustaine, and F. Dentener (2004), Global modeling of heterogeneous chemistry on mineral aerosol surfaces: Influence on tropospheric ozone chemistry and comparison to observations, *J. Geophys. Res.*, *109*, D02304, doi:10.1029/2003JD003868.

Bertschi, I. T., and D. A. Jaffe (2005), Long-range transport of ozone, carbon monoxide, and aerosols to the NE Pacific troposphere during the summer of 2003: Observations of smoke plumes from Asian boreal fires, *J. Geophys. Res.*, *110*, D05303, doi:10.1029/2004JD005135.

Boucher, O., and D. Tanré (2000), Estimation of the aerosol perturbation to the Earth's radiative budget over oceans using POLDER satellite retrievals, *Geophys. Res. Lett.*, *27*, 1103–1106.

Boucher, O., M. Pham, and C. Venkataraman (2002), Simulation of the atmospheric sulfur cycle in the Laboratoire de Météorologie Dynamique General Circulation Model. Model description, model evaluation, and global and European budgets, *Notes Sci.*, *23*, Inst. Pierre Simon Laplace, Paris.

Bréon, F.-M., D. Tanré, and S. Generoso (2002), Aerosol effect on cloud droplet size monitored from satellite, *Science*, *295*, 834–838.

Carmichael, G. R., M.-S. Hong, H. Ueda, L.-L. Chen, K. Murano, J.-K. Park, H. Lee, Y. Kim, C. Kang, and S. Shim (1997), Aerosol composition at Cheju Island, Korea, *J. Geophys. Res.*, *102*, 6047–6061.

Chen, L.-L., et al. (1997), Influence of continental outflow events on the aerosol composition at Cheju Island, South Korea, *J. Geophys. Res.*, *102*, 28,551–28,574.

Chiapello, I., P. Goloub, D. Tanré, A. Marchand, J. Herman, and O. Torres (2000), Aerosol detection by TOMS and POLDER over oceanic regions, *J. Geophys. Res.*, *105*, 7133–7142.

Chuang, P. Y., R. M. Duvall, M. S. Bae, A. Jefferson, J. J. Schauer, H. Yang, J. Z. Yu, and J. Kim (2003), Observations of elemental carbon and absorption during ACE-Asia and implications for aerosol radiative properties and climate forcing, *J. Geophys. Res.*, *108*(D23), 8634, doi:10.1029/2002JD003254.

Chun, Y., K.-O. Boo, J. Kim, S.-O. Park, and M. Lee (2001), Synopsis, transport, and physical characteristics of Asian dust in Korea, *J. Geophys. Res.*, *106*, 18,461–18,469.

Claquin, T. (1999), Modélisation de la minéralogie et du forçage radiatif des poussières désertiques, Ph.D. thesis, 154 pp., Univ. Paris VI, Paris.
Clarke, A. D., and J. Noone (1985), Measurements of soot aerosol in Arctic snow, *Atmos. Environ.*, *19*, 2045–2054.
Clerbaux, C., J. Hadji-Lazaro, D. Hauglustaine, and G. Mégie (2001), Assimilation of carbon monoxide measured from satellite in a three-dimensional chemistry-transport model, *J. Geophys. Res.*, *106*, 15,385–15,394.
Collins, W. D., P. J. Rasch, B. E. Eaton, B. V. Khattatov, J. F. Lamarque, and C. S. Zender (2001), Simulating aerosols using a chemical transport model with assimilation of satellite aerosol retrievals: Methodology for INDOEX, *J. Geophys. Res.*, *106*, 7313–7336.
Collins, W. D., P. J. Rasch, B. E. Eaton, D. W. Fillmore, J. T. Kiehl, C. T. Beck, and C. S. Zender (2002), Simulation of aerosol distributions and radiative forcing for INDOEX: Regional climate impacts, *J. Geophys. Res.*, *107*(D19), 8028, doi:10.1029/2000JD000032.
Courtier, P., J. N. Thepaut, and A. Hollingsworth (1994), A strategy for operational implementation of 4D-Var, using an incremental approach, *Q. J. R. Meteorol. Soc.*, *120*, 1389–1408.
Damoah, R., N. Spichtinger, C. Forster, P. James, I. Mattis, U. Wandinger, S. Beirle, T. Wagner, and A. Stohl (2004), Around the world in 17 days—Hemispheric-scale transport of forest fire smoke from Russia in May 2005, *Atmos. Chem. Phys.*, *4*, 1311–1321.
Deschamps, P.-Y., F.-M. Bréon, M. Leroy, A. Podaire, A. Bricaud, J.-C. Buriez, and G. Sèze (1994), The POLDER mission: Instrument characteristics and scientific objectives, *IEEE Trans. Geosci Remote Sens.*, *32*, 598–615.
Deuzé, J. L., P. Goloub, M. Herman, A. Marchand, G. Perry, S. Susanna, and D. Tanré (2000), Estimate of the aerosol properties over the ocean with POLDER, *J. Geophys. Res.*, *105*, 15,329–15,346.
Deuzé, J. L., et al. (2001), Remote sensing of aerosols over land surfaces from POLDER-ADEOS-1 polarized measurements, *J. Geophys. Res.*, *106*, 4913–4926.
Diner, D. J., et al. (1998), Multi-angle Imaging SpectroRadiometer (MISR) description and experiment overview, *IEEE Trans. Geosci. Remote Sens.*, *36*, 1072–1087.
Dubovik, O., and M. D. King (2000), A flexible inversion algorithm for retrieval of aerosol optical properties from sun and sky radiance measurements, *J. Geophys. Res.*, *105*, 20,673–20,696.
Dubovik, O., A. Smirnov, B. N. Holben, M. D. King, Y. J. Kaufman, T. F. Eck, and I. Slutsker (2000), Accuracy assessments of aerosol optical properties retrieved from Aerosol Robotic Network (AERONET) sun and sky radiance measurements, *J. Geophys. Res.*, *105*, 9791–9806.
Fisher, M., and D. J. Lary (1995), Lagrangian 4-dimensional variational data assimilation of chemical-species, *Q. J. R. Meteorol. Soc.*, *121*, 1681–1704.
Generoso, S. (2004), Etude des interactions entre aerosols et climat: Assimilation des observations spatiales de POLDER dans LMDz-INCA, Ph.D. thesis, 182 pp., Univ. Paris VII, Denis Diderot, Paris. (Available at http://tel.archives-ouvertes.fr/documents/archives0/00/00/84/56/index.html)
Generoso, S., F.-M. Bréon, Y. Balkanski, O. Boucher, and M. Schulz (2003), Improving the seasonal cycle and interannual variations of biomass burning aerosol sources, *Atmos. Chem. Phys.*, *3*, 1211–1222.
Gérard, B., J.-L. Deuzé, M. Herman, Y. J. Kaufman, P. Lallart, C. Oudard, L. A. Remer, B. Roger, B. Six, and D. Tanré (2005), Comparisons between POLDER 2 and MODIS/Terra aerosol retrievals over ocean, *J. Geophys. Res.*, *110*, D24211, doi:10.1029/2005JD006218.
Gerber, H. (1991), Supersaturation and droplet spectral evolution in fog, *J. Atmos. Sci.*, *48*, 2569–2588.
Goloub, P., and O. Arino (2000), Verification of the consistency of POLDER aerosol index over land with ATSR-2/ERS-2 fire product, *Geophys. Res. Lett.*, *27*, 899–902.
Guelle, W., M. Schulz, Y. Balkanski, and F. Dentener (2001), Influence of the source formulation on modeling the atmospheric global distribution of sea salt aerosol, *J. Geophys. Res.*, *106*, 27,509–27,524.
Guibert, S., M. Volker, M. Schulz, J. Bösenberg, R. Eixmann, I. Mattis, G. Pappalardo, M. R. Perrone, N. Spinelli, and G. Vaughan (2005), The vertical distribution of aerosol over Europe—Synthesis of one year of EARLINET aerosol lidar measurements and aerosol transport modeling with LMDz-INCA, *Atmos. Environ.*, *39*, 2933–2943.
Hakami, A., D. K. Henze, J. H. Seinfeld, T. Chai, Y. Tang, G. R. Carmichael, and A. Sandu (2005), Adjoint inverse modeling of black carbon during the Asian Pacific Regional Aerosol Characterization Experiment, *J. Geophys. Res.*, *110*, D14301, doi:10.1029/2004JD005671.
Hauglustaine, D. A., F. Hourdin, L. Jourdain, M.-A. Filiberti, S. Walters, J.-F. Lamarque, and E. A. Holland (2004), Interactive chemistry in the Laboratoire de Météorologie Dynamique general circulation model: Description and background tropospheric chemistry evaluation, *J. Geophys. Res.*, *109*, D04314, doi:10.1029/2003JD003957.
Herber, A., L. W. Thomason, H. Gernandt, U. Leiterer, D. Nagel, K. Schulz, J. Kaptur, T. Albrecht, and J. Notholt (2002), Continuous day and night aerosol optical depth observations in the Arctic between 1991 and 1999, *J. Geophys. Res.*, *107*(D10), 4097, doi:10.1029/2001JD000536.
Herman, M., J.-L. Deuzé, A. Marchand, B. Roger, and P. Lallart (2005), Aerosol remote sensing from POLDER/ADEOS over the ocean: Improved retrieval using a nonspherical particle model, *J. Geophys. Res.*, *110*, D10S02, doi:10.1029/2004JD004798.
Holben, B. N., et al. (1998), AERONET—A federated instrument network and data archive for aerosol characterization, *Remote Sens. Environ.*, *66*, 1–16.
Hourdin, F. D., and A. Armengaud (1999), The use of finite volume methods for atmospheric advection of trace species. Part I: Test of various formulations in a general circulation model, *Mon. Weather Rev.*, *127*, 822–837.
Intergovernmental Panel on Climate Change (2001), *Climate Change 2001: The Scientific Basis—Contribution of Working Group I to the Third Assessment Report of the Intergovernmental Panel on Climate Change*, 881 pp., Cambridge Univ. Press, New York.
Jaffe, D., I. Bertschi, L. Jaeglé, P. Novelli, J. S. Reid, H. Tanimoto, R. Vingarzan, and D. L. Westphal (2004), Long-range transport of Siberian biomass burning emissions and impact on surface ozone in western North America, *Geophys. Res. Lett.*, *31*, L16106, doi:10.1029/2004GL020093.
Kalman, R., and R. Bucy (1961), New results in linear filtering and prediction theory, *J. Basic Eng.*, *83*, 95–108.
Kaufman, Y. J., D. Tanré, and O. Boucher (2002), A satellite view of aerosols in the climate system, *Nature*, *419*, 215–223.
Kaufman, Y. J., O. Boucher, D. Tanré, M. Chin, L. A. Remer, and T. Takemura (2005), Aerosol anthropogenic component estimated from satellite data, *Geophys. Res. Lett.*, *32*, L17804, doi:10.1029/2005GL023125.
Khattatov, B. V., J. C. Gille, L. V. Lyjak, G. P. Brasseur, V. L. Dvorstov, A. E. Roche, and J. W. Waters (1999), Assimilation of photochemically active species and a case analysis of UARS data, *J. Geophys. Res.*, *104*, 18,715–18,737.
Koch, D., and J. Hansen (2005), Distant origins of Arctic black carbon: A Goddard Institute for Space Studies ModelE experiment, *J. Geophys. Res.*, *110*, D04204, doi:10.1029/2004JD005296.
Lacis, A. A., and M. I. Mishchenko (1994), Climate forcing, climate sensitivity, and climate response: A radiative modeling perspective on atmospheric aerosols, in *Aerosol Forcing of Climate*, edited by R. J. Charlson and J. Heintzenberg, pp. 11–42, John Wiley, Hoboken, N. J.
Lamarque, J. F., B. V. Khattatov, J. C. Gille, and G. P. Brasseur (1999), Assimilation of Measurement of Air Pollution from Space (MAPS) CO in a global three-dimensional model, *J. Geophys. Res.*, *104*, 26,209–26,218.
Le Dimet, F.-X., and O. Talagrand (1986), Variational algorithms for analysis and assimilation of meteorological observations: Theoretical aspects, *Tellus, Ser. A*, *38*, 97–110.
Liousse, C., J. E. Penner, C. Chuang, J. J. Walton, H. Eddleman, and H. Cachier (1996), A global three-dimensional model study of carbonaceous aerosols, *J. Geophys. Res.*, *101*, 19,411–19,432.
Lorenc, A. C., R. S. Bell, and B. Macpherson (1991), The Meteorological Office Analysis Correction Data Assimilation scheme, *Q. J. R. Meteorol. Soc.*, *117*, 59–89.
Ménard, R., S. E. Cohn, L.-P. Chang, and P. M. Lyster (2000), Assimilation of stratospheric chemical tracer observations using a Kalman filter. Part I: Formulation, *Mon. Weather Rev.*, *128*, 2654–2671.
Myhre, G., et al. (2004), Intercomparison of satellite retrieved aerosol optical depth over the ocean, *Bull. Am. Meteorol. Soc.*, *61*, 499–513.
Nedelec, P., V. Thouret, J. Brioude, B. Sauvage, J.-P. Cammas, and A. Stohl (2005), Extreme CO concentrations in the upper troposphere over northeast Asia in June 2003 from the in situ MOZAIC aircraft data, *Geophys. Res. Lett.*, *32*, L14807, doi:10.1029/2005GL023141.
Quaas, J., and O. Boucher (2005), Constraining the first aerosol indirect radiative forcing in the LMDZ GCM using POLDER and MODIS satellite data, *Geophys. Res. Lett.*, *32*, L17814, doi:10.1029/2005GL023850.
Quaas, J., O. Boucher, and F.-M. Bréon (2004), Aerosol indirect effects in POLDER satellite data and the Laboratoire de Météorologie Dynamique–Zoom (LMDZ) general circulation model, *J. Geophys. Res.*, *109*, D08205, doi:10.1029/2003JD004317.
Rasch, P. J., N. M. Mahowald, and B. E. Eaton (1997), Representations of transport, convection and the hydrological cycle in chemical transport models: Implications for the modeling of short-lived and soluble species, *J. Geophys. Res.*, *102*, 28,127–28,138.
Rasch, P. J., W. D. Collins, and B. E. Eaton (2001), Understanding the Indian Ocean experiment (INDOEX) aerosol distributions with an aerosol assimilation, *J. Geophys. Res.*, *106*, 7337–7355.
Rinke, A., K. Dethloff, and M. Fortmann (2004), Regional climate effects of Arctic Haze, *Geophys. Res. Lett.*, *31*, L16202, doi:10.1029/2004GL020318.

Rodgers, C. D. (2000), *Inverse Method for Atmospheric Sounding: Theory and Practice*, World Sci., Hackensack, N. J.

Schulz, M., Y. J. Balkanski, W. Guelle, and F. Dulac (1998), Role of aerosol size distribution and source location in a three-dimensional simulation of a Saharan dust episode tested against satellite-derived optical thickness, *J. Geophys. Res.*, *103*, 10,579–10,592.

Schulz, M., G. de Leeuw, and Y. Balkanski (2003), Sea-salt aerosol source functions and emissions, in *Emission of Atmospheric Trace Compounds*, edited by C. Granier, P. Artaxo, and C. E. Reeves, pp. 347–372, Springer, New York.

Shaw, G. E. (1995), The Arctic haze phenomenon, *Bull. Am. Meteorol. Soc.*, *76*, 2403–2412.

Smirnov, A., B. N. Holben, T. Eck, O. Dubovik, and I. Slutsker (2000), Cloud screening and quality control algorithms for the AERONET data base, *Remote Sens. Environ.*, *73*, 337–349.

Stowe, L. L., A. M. Ignatov, and R. R. Singh (1997), Development, validation, and potential enhancements to the second-generation operational aerosol product at the National Environmental Satellite, Data, and Information Service of the National Oceanic and Atmospheric Administration, *J. Geophys. Res.*, *102*(D14), 16,923–16,934.

Talagrand, O. (2002), A posteriori validation of assimilation algorithms, in *Data Assimilation for the Earth System*, edited by R. Swinbank, V. Shutyaev, and W. A. Lahoz, pp. 85–95, Springer, New York.

Tanré, D., F.-M. Bréon, J. L. Deuzé, M. Herman, P. Goloub, F. Nadal, and A. Marchand (2001), Global observation of anthropogenic aerosols from satellite, *Geophys. Res. Lett.*, *28*, 4555–4558.

Tegen, I., and A. Lacis (1996), Modeling of particle size distribution and its influence on the radiative properties of mineral dust aerosol, *J. Geophys. Res.*, *101*, 19,237–19,244.

Tiedtke, M. (1989), A comprehensive mass flux scheme for cumulus parametrization in large-scale models, *Mon. Weather Rev.*, *117*, 1779–1800.

Van Leer, B. (1977), Towards the ultimate conservative difference scheme. Part IV: A new approach to numerical convection, *J. Comput. Phys.*, *23*, 276–299.

Yamanouchi, T., et al. (2005), Arctic Study of Tropospheric Aerosol and Radiation (ASTAR) 2000: Arctic haze case study, *Tellus, Ser. B*, *57*, 141–152.

Y. Balkanski, F.-M. Bréon, F. Chevallier, and M. Schulz, Institut Pierre-Simon Laplace/Laboratoire des Sciences du Climat et de l'Environnement, Commissariat à l'Énergie Atomique–Centre National de la Recherche Scientifique, F-91191 Gif-sur-Yvette, France.

I. Bey and S. Generoso, Laboratoire de Modélisation de la Chimie Atmosphérique, Ecole Polytechnique Fédérale de Lausanne, CH-1015 Lausanne, Switzerland. (sylvia.generoso@epfl.ch)